Accelerated Stress Testing of SiC MEMS-DCA Pressure Transducers

Ender Savrun[1], Vu Nguyen[1], Robert Okojie[2], and Charles Blaha[3]

[1]Sienna Technologies, Inc., 19501 144th Avenue NE, Suite F-500, Woodinville, WA 98072
Phone: (425) 485-7272; E-mail: ender.savrun@siennatech.com
[2]NASA Glenn Research Center, 21000 Brookpark Road, Mail-Stop 77-1, Cleveland OH 44135
Phone: (216) 433-6522; E-mail: robert.s.okojie@nasa.gov
[3]Akima Corporation, 22021 Brookpark Road, Fairview Park, OH 44126

Abstract

Preliminary accelerated stress tests (AST) have been performed on 6H-SiC pn-junction piezoresistive pressure transducers that were packaged by Microelectromechanical Systems Direct Chip Attach (MEMS-DCA) process for the purpose of evaluating their long-term operational stability and reliability under cyclic pressure and temperature. Finite element analysis (FEA) was used to understand the stress distribution at critical sensor/Aluminum nitride (AlN) header and AlN header/Kovar interfaces and to develop design strategies that minimize the thermomechanical stresses. The thermomechanical stresses that are inherent in traditional pressure transducer packaging methods were significantly reduced by matching via material selection the coefficient of thermal expansion (CTE) between the SiC sensor and the AlN header and also mechanically de-coupling the sensor from the usually high CTE metal casing. This resulted in achieving thermal stability and reproducibility of critical transducer parameters such as the zero offset, sensitivity, and resistance.

Keywords: Accelerated Stress Test, AlN, High Temperature, MEMS, Pressure Sensor, Silicon Carbide.

Introduction

There is a growing demand for pressure transducers that can operate reliably at temperatures ranging between 300 and 600ºC. Pressure monitoring during deep well drilling and combustion in aeronautical and automobile engines require pressure transducers that can operate in this range of temperature [1]. There is also a growing demand for improved fuel efficiency in jet engines and automobiles as well as the reduction of undesirable emission of hydrocarbons and other combustion by-products such as NOx and CO [2]. However, it has remained a challenge to apply conventional semiconductor sensing devices because they are limited to operating temperatures less than 300ºC due to the limitations imposed by their material properties, packaging technology, and design constraints. In cases where they are utilized at higher temperature, extensive and expensive packaging methods such as plumbing for water cooling are adopted. Sensor on insulator (SOI) technology has long been adopted to further extend the operational capability of pressure sensor to temperatures beyond 300ºC [3]. While the SOI based sensors can be utilized for short duration instrumentation, their long term stability and reliability remain a challenge. Silicon carbide (SiC) has long been viewed as a potentially useful semiconductor for high temperature applications. SiC-based sensors have been demonstrated to operate at temperatures up to 600ºC [4,5], thereby offering promise of direct insertion into the high temperature environment without the need for cooling. However, the absence of reliable packaging methodologies for such extreme temperatures has largely prevented the application of SiC sensors. Devices capable of functioning in these harsh environments need the appropriate package to sustain operation throughout their operational life.

The identified failure mechanism is associated with the changes in resistance at the metallurgical junction between sensor and the wire bonds due to reaction kinetics that eventually weaken the bond [6]. Another prominent failure mechanism is the fatigue induced sensor cracking due to the thermomechanical stress between the sensor and the package components as a result of mismatches in the CTEs [7].

Over the past two years, Sienna Technologies, Inc. has supported the implementation of a robust high temperature SiC MEMS pressure transducer that is based on MEMS-DCA developed at NASA Glenn Research Center [8]. The MEMS-

DCA is based on direct chip attach methodology, thus eliminating wire bonds and the associated failures mechanisms. It also de-couples the CTE mismatches between the sensor and surrounding package components, thereby minimizing the thermomechanical stress between sensor and package components.

High Temperature Microsystems Packaging Issues

The most critical issues in designing electronic packages for Microsystems for high temperature applications are (*i*) mitigation of thermal stresses caused by the CTE mismatches between the devices and various package elements (including substrates), (*ii*) thermal shock resistance brought about by thermal cycling during service, (*iii*) chemical stability and compatibility between the various package elements most (notably contact metallurgies), and (*iv*) heat dissipation to keep the temperatures at safe operating levels. Material properties can significantly impact how well the package can meet the requirements. Therefore, the package design is to a great extent, influenced by the available materials.

A survey of current packaging materials suggests that AlN is an ideal candidate for packaging SiC-devices for high-temperature (600°C) applications [9]. Some of the important advantages of AlN include high thermal conductivity (200 $W \bullet m^{-1} \bullet K^{-1}$), which decreases only slightly with increasing temperature; a CTE (4.1 x 10^{-6}°C^{-1}) that closely matches that of SiC (3.7 x 10^{-6}°C^{-1}), which minimizes the thermal stresses; good thermal shock resistance and environment stability at high temperatures; non-toxicity (unlike beryllia); high electrical resistivity; high mechanical strength; and chemical inertness at high temperatures.

Wire bonds are known to be the weakest links in a package that operates at high temperatures. The wires can fail by creep deformation at high temperatures. They can form unwanted intermetallics with the bond pad materials thereby weakening the wire bond interface.

Stress Analysis of the Package

In earlier works, more attention was focused on proof of concept demonstration of SiC pressure sensor operation at 600ºC than on the effect of thermomechanical stress and its impact on mechanical and electrical sensor functionality and long-term reliability [4,5]. While the first generation high temperature MEMS-DCA offered the promise of supporting sensor operation at 600ºC and beyond, it was still hindered by the undesirable thermomechanical coupling between sensor and package components [5].

A second generation MEMS-DCA packaging as shown in cross section in Figure 1 was developed and used for packaging the SiC sensors reported in this paper [8]. The cross section depicts the primary components of the transducer and the several unique characteristics that combine to provide its robustness. The AlN is selected because its coefficient of thermal expansion (CTE), α_{AlN} = 4.1 ppm/ºC matches closely to that of SiC of α_{SiC} = 3.7 ppm/ºC. The CTE of the specially developed sealing glass also matches very close to that of SiC. The SiC sensor is housed in an AlN header and sealed with the glass to achieve a leak rate of better than 10^{-7} l-atm-s^{-1} He. When the sensor is placed on the circular cavity of the AlN receptacle, as shown in Figure 1, only the sensor's circular diaphragm is free to deflect in and out of the reference cavity. The sealing glass is applied into the narrow gap (< 100 μm) between the SiC sensor and AlN. The bond pads of the sensor align precisely with the holes in the AlN so that the wires that are inserted in these holes intimately contact the bond pads.

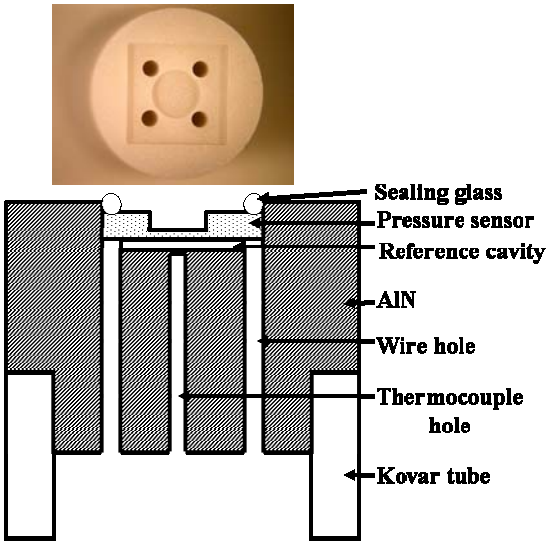

Figure 1: Cross sectional and top views of the MEMS-DCA depicting unique advantages and novelty: direct wire contact eliminates wire bonding; higher density chip count on wafer; thermomechanical stress de-coupling of sensor from metal tube minimizes instability; thermocouple access provides for temperature measurement for compensation and calibration purposes.

The stresses brought about by thermal cycling during service can induce fatigue at several critical areas of the system such as glass sealing/sensor and sensor/AlN interfaces. Therefore, to optimize the new package design concept, a non-linear finite element analysis (FEA) was conducted to establish the influence of the length of AlN cylinder on the stresses and deformation developing near the braze and the sensor surface. All parts of the assembly are modeled utilizing ANSYS SOLID45 eight node brick elements [10]. The contact between AlN cylinder and the bottom of the SiC is modeled by employing CONTA173 and TARGE170 elements. The non-linear solution procedure involves a two-step temperature loading. The non-linearity arises from the presence of the contact surface between the chip and the cylinder. By taking advantage of the symmetry of the structure as shown in Figure 2a, a quarter of the assembly was modeled. Consequently, the symmetry displacement boundary conditions were imposed to the appropriate sides of the components.

The results are depicted in terms of first principal and equivalent stress distributions near the AlN/Kovar braze joint and the AlN/SiC interface. In the FEA, the thermal loading applied in two steps begins with 850ºC, the temperature at which the AlN is brazed to the Kovar tube, then reduces to 650ºC, the temperature at which the glass is applied to the SiC sensor, and finally to 25ºC. The distribution of the first principal and equivalent stresses in the layer of the SiC elements that is in contact with AlN cylinder is shown in Figures 2b and 2c, respectively. By varying the length to the AlN cylinder, the maximum stress values seen at the edge of the SiC sensor remained unchanged at about 400 MPa (principal) and 652 MPa (equivalent).

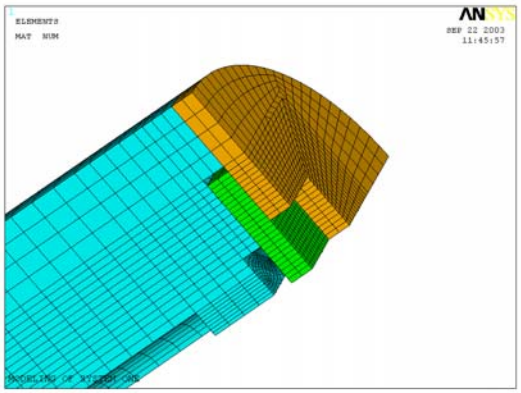

Figure 2a: Quarter symmetry model of the MEMS-DCA used for the analysis depicts the SiC chip sandwiched between the glass layer and the AlN cylinder.

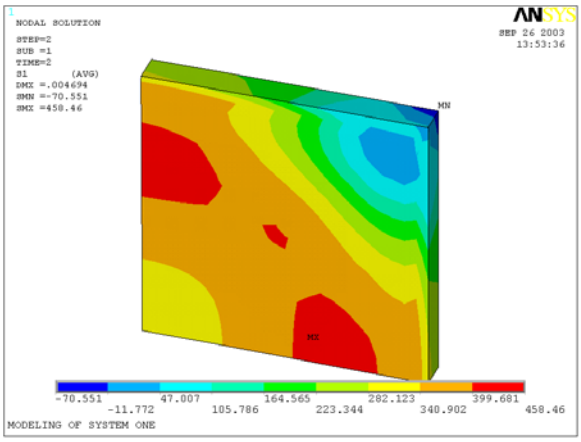

Figure 2b: The distribution of the first principal stress (MPa) in the layer of SiC elements that is in contact with AlN cylinder (AlN header – 25.4 mm).

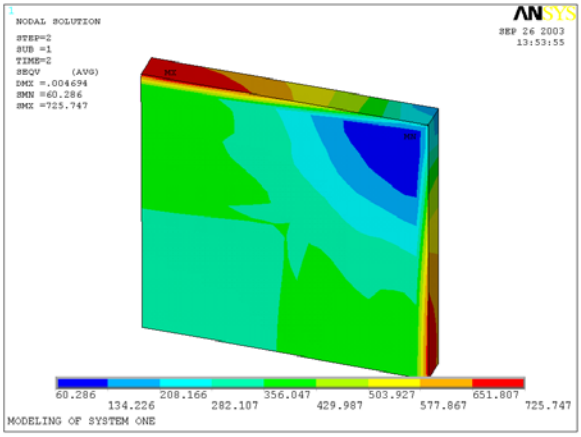

Figure 2c: The distribution of the equivalent stress (MPa) in the layer of SiC elements that is in contact with AlN cylinder (AlN header – 25.4 mm).

The gap, penetration, and pressure arising from the contact between AlN cylinder and SiC chip are presented hereafter. Figure 3a shows the modeled cavity surface along which the AlN cylinder is in contact with the SiC chip and is used for further reference. The distribution of the pressure arising from the contact between the AlN cylinder and SiC chip is shown in Figure 3b. As expected, the maximum contact pressure develops near the middle of the SiC chip sides. In the broader context of the analysis, no considerable variation of the pressure is observed because of the different lengths of the AlN cylinder. The influence of the AlN cylinder length on the values of these stresses was found to be negligible.

By this analysis, design optimization of the distance between the SiC sensor and the Kovar metal tube ensures that the large thermomechanical stress that the Kovar induces on the AlN does not affect the sensor. Therefore, the only strains coupled to the sensor are generated at the SiC/glass and SiC/AlN interfaces. Thus, the de-coupling of the sensor from the metal tube is effectively achieved by this design.

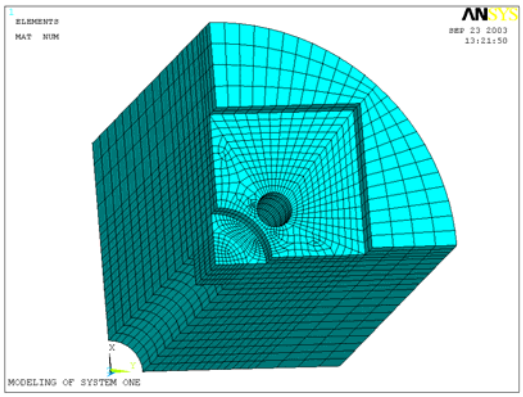

Figure 3a. Close view of contact area in AlN cylinder.

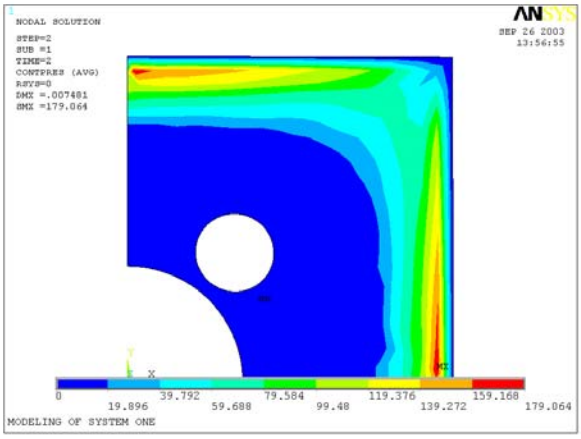

Figure 3b: Variation of contact pressure (MPa) (AlN cylinder – 25.4 mm).

Transducer Parametric Analysis

The resistors were arranged in a Wheatstone bridge configuration shown in Figure 4, which will have a zero bridge output voltage, V_{oz}, if the four resistor elements are exactly the same (full bridge symmetry). Deviation from symmetry may be the result of factors such as non uniformity in the sheet resistance across the epilayer in which the resistors were fabricated, process induced structural non uniformity during fabrication, and non uniformity in the contact resistance and the contact wires. Another possible influence on the V_{oz} is the thermomechanical stress transmitted to the sensor by the package components.

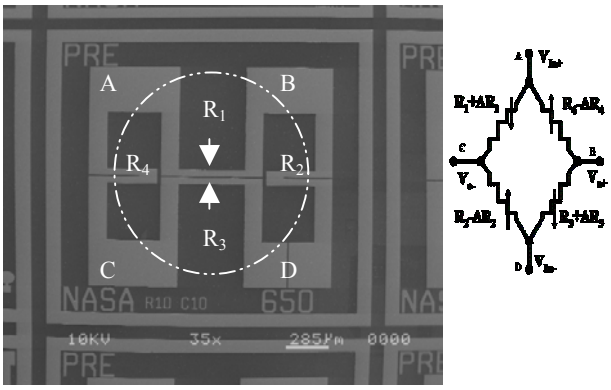

Figure 4: Scanning electron microphotograph of the top view of a SiC pressure sensor shows the four resistors. Contact pads A-D and the outline of the circular diaphragm on the backside are also shown. On the right is the Wheatstone bridge equivalent circuit.

In the transducers under discussion, the bridge circuit is asymmetric. Therefore, in a closed bridge condition, the output is obtained as:

$$V_{oz} = V_{in}\frac{1}{2}\left(\frac{R_2 - R_1}{R_1 + R_2} + \frac{R_4 - R_3}{R_3 + R_4}\right) \qquad (1)$$

and the output resistance is resolved to be

$$R_o = \left(\frac{(R_2 + R_3)(R_1 + R_4)}{R_1 + R_2 + R_3 + R_4}\right) \qquad (2)$$

Due to asymmetry, the bridge output, V_{oz}, under unstrained condition is non-zero. When pressure is applied to the diaphragm, each resistor experiences a strain that corresponds to the applied pressure. The relative change in each resistor element due to strain is generally expressed as:

$$\Delta R = R\varepsilon G \qquad (3)$$

where G represents the gauge factor (strain sensitivity factor), ε is the strain corresponding to the pressure applied. The TCR of a resistor, denoted as β (ppm/°C), determines the resistor value at given temperature. This can be expressed as:

$$R_T = R_o(1 + \beta\Delta T) \qquad (4)$$

where R_T (Ω) is the resistance at temperature, R_o is the resistance at room temperature, and ΔT (°C) is the change in temperature from the reference temperature (usually room temperature). The temperature effect of the gauge factor, (strain sensitivity) is expressed as:

$$G_T = G_o(1 + \gamma\Delta T) \quad (5)$$

where γ is the temperature coefficient of gauge factor (ppm/ºC) [(i.e. temperature coefficient of sensitivity (TCS)], G_T is the gauge factor at temperature and G_o is the gauge factor at room temperature.

Under an unstrained condition (no applied pressure and sensor not packaged), the bridge output is governed only by equations (1), (2), and (4), from which the unstrained zero offset, V_{oz}, is obtained. After the sensor is attached to the package at elevated temperature (~650ºC) and cooled down to room temperature, it experiences a residual strain due to the mismatch in the CTE between sensor and the AlN header. Thus with the sensor packaged and no external pressure applied, it is in a strained state with a residual stress, δ. Therefore, the effect of the mismatch on each resistance causes equation (3) to be modified as:

$$\Delta R_\varepsilon(T) = R_o G_o \left[1 + (\beta + \gamma)\Delta T + \gamma\beta(\Delta T)^2\right](\varepsilon + \delta) \quad (6)$$

On the basis of equation (6), the output resistance measured across the bridge of a fully packaged sensor is in fact the combined effects of β, γ, and δ. The implication of equation (6) is that as the temperature increases, the residual strain, δ, approaches zero and the resistance becomes governed purely by β *and* γ parameters.

From the above analysis, it is seen that equation (6) is important for understanding the behavioral characteristics of the transducer and forms the basis of temperature compensation. It also reveals the effect of thermomechanical stress on the system and its deleterious effect on the stability of the output. The MEMS-DCA packaging scheme adopted in this work is a deliberate attempt to minimize this problem. The choice of packaging material with regard to how closely the CTEs are matched is such that the coupled stress is significantly minimized and the drift and shift reduced.

Transducer Accelerated Stress Tests Protocol

Six SiC transducers were selected for the accelerated stress test that was used to evaluate the SiC transducers is described below. After the sensor is fully packaged, a helium leak test is performed to determine the leak rate through the sealing glass. In almost all cases, the leak rate ranged between 10^{-9} and 10^{-6} l-atm-s^{-1} He. The transducer is then heated in an atmospheric oven at 10ºC/min and held to dwell at a temperature that was above its rated operating temperature (criteria for rating discussed later) for three hours while pressurized at 100 psi. The transducer is then cooled at –2ºC/min to room temperature and the pressure removed after cooling down. The measured bridge zero offset voltage, V_{oz}, (no external pressure applied) at room temperature after this step was then used as the reference (we call this V_{ozref}) to measure deviations of the V_{oz} in subsequent measurements. Next, pressure was applied at room temperature to 100 psi in 10 psi steps during the upward and downward pressure excursions. Twenty-one cycles of these pressure excursions were performed specifically to quantify the hysterisis, non-linearity, and any shift in the offset. The temperature is raised to 100ºC, held for three hours, and then the above mentioned twenty-one cycles of pressurization sequence is repeated. The sequence is repeated again at selected temperatures until the highest operating temperature was reached when pronounced instability in the output was observed. Finally, the transducer was then cooled down to room temperature and the final pressurization cycles were performed to end the run. The result of the 21st AST runs at each temperature was recorded and plotted and shown in Figure 5. It is worth noting that all the preceding AST cycles tracked very well with the 21st cycle and thus it was not necessary to plot them.

Results

Thermal Leakage Current

The choice of the soak temperature was based on the degree of bridge output instability induced by the thermally generated pn-junction leakage current for a input voltage, V_{in}, of 5 V. As temperature increases, the thermally generated carriers are transported into the conduction band and are swept by the external electric field (i.e., V_{in}) to become part of the current transport. A qualitative determination of effect of this leakage current is made by dropping V_{in} to 2 V. The reduced electric field reduced the output instability to a manageable level until a higher temperature is reached at which more carriers are either generated or phonon scattering mechanism begins to dominate the carrier transport process [11,12].

For this batch of transducers, the preliminary temperature excursion to higher temperature indicated pronounced V_{oz} instability at 400ºC, for a V_{in} of 5 V. By reducing the V_{in} to 2 V, stability was achieved at 600ºC. However, the main goal of this work was to initiate a systematic evaluation from 300ºC.

For the SiC piezoresistive sensors under discussion, the substrate was aluminum doped p-type 6H-SiC on which a 2 μm thick nitrogen doped n-type layer was homoepitaxially grown [13]. To minimize such undesirable thermally generated carriers, it is preferred that the epilayer be of high quality with optimized resistivity and the p-type SiC substrate be

of very high resistivity and quality. As the impurity concentration in the n-type epilayer and the p-type is increased and decreased, respectively, the junction leakage current will decrease correspondingly, thus allowing the transducer stable operation to be extended to higher temperatures. In this preliminary AST work, however, the p-type substrate has high defect density and un-optimized resistivity (ρ = 1.9 Ω-cm, N_a = 3.25 x 10^{18} cm^{-3}) on which the epilayer having impurity concentration of 6.2 x 10^{18} cm^{-3} was grown.

Thermal Stability of the Zero Offset, V_{oz}

As stated earlier, the relatively low doping level of the p-type substrate results in a high thermal junction leakage current that limited stable operating temperature to 300 °C for V_{in} = 5 V. In Figure 5, the net full-scale output (FSO) voltage as function of cyclic pressure and temperature is shown, which depicts the characteristic drop in FSO common in piezoresistive sensors as temperature is increased [4,14]. The solid and symbol plots represent the 21st 0-100 psi and 100-0 psi pressure cycles at each increasing temperature excursion, respectively. The dash and symbol plots also represent similar cycles during the cooling down sequence.

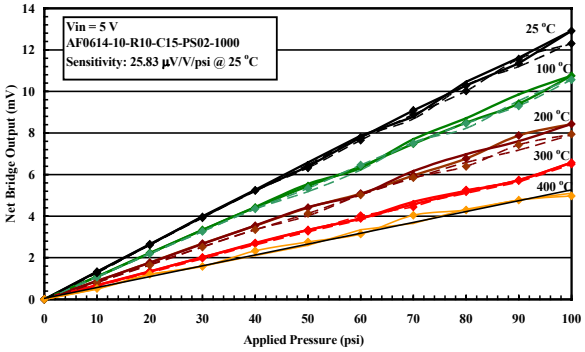

Figure 5: Dynamic output voltage as function of pressure at different temperature after extensive ASTs shows the degree of repeatability, hysterisis and linearity. The solid/solid-symbol plots represent the 21st 0-100 psi and 100-0 psi pressure cycles at each increasing temperature excursion. The dash/dash-symbol plots represent the similar cycles during the cooling down sequence.

Figure 6a shows the V_{orefz} (at zero applied pressure) after the first set of thermal cycles described above. During excursion to higher temperature, the V_{oz} followed a non-linear decrease to 400ºC. Due to the leakage current and the instability introduced at 400ºC as explained earlier, the temperature was decreased to 300ºC and cooled down. It is seen that the slopes of the two plots tracked each other, albeit with a V_{oz} shift of about 1.86 mV between the heating and cooling regimes. This result clearly indicated an undesirable drift in the V_{oz}, since both plots were not superimposed on each other. In the parametric analysis presented earlier, equation (6) is determined to be an important to the reliability of the transducer because any irreversible change in the resistance as a result of the permanent changes in the β and γ parameters will reproduced a corresponding change in the V_{oz} [i.e. equation (1)].

To determine the extent of the observed drift in V_{oz}, a time dependent evaluation was performed. In this case, no pressure was applied and the transducer was heated to 300ºC and held for several hours. The V_{oz} was recorded over time at this temperature and also recorded during intermittent cooling downs. This cycle was repeated for several hours and the result is shown in Figure 6b. It can be seen that the several measured V_{oz} (25ºC, time) did not drift by more than 0.5 mV from the room temperature V_{ozref}. Similarly, the V_{oz} (300ºC, time), did not drift more than 0.6 mV from V_{ozref} at 300ºC. This implied that the temperature coefficient of offset (TCO) is stable. It also indicated that the drift that was observed during the maiden set of AST runs (e.g. see Figure 6a) was due to the transducer undergoing stabilization (i.e. burn-in).

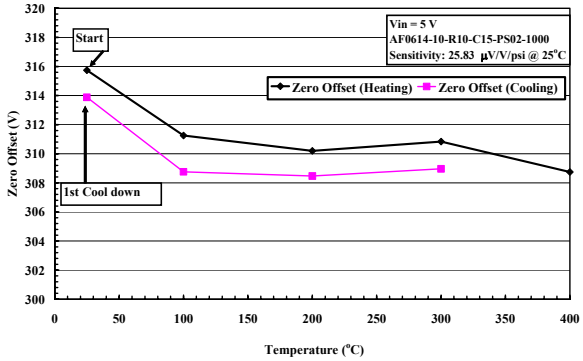

Figure 6a: Representative shift in unstrained zero offset the maiden set of AST runs.

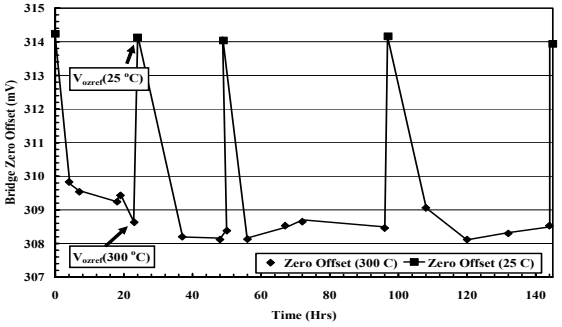

Figure 6b: Representative unstrained zero offset after 130-hrs of soaking at 300ºC and cooling down.

The reliability of a sensing device and the accuracy of the temperature compensation scheme are largely governed by the stability of the TCO after the initial calibration. To properly calibrate a Wheatstone bridge based piezoresistive pressure transducer, such as the one under discussion here, it is crucial that the V_{oz} at room temperature and the maximum rated temperature remain unchanged from its fixed values after stabilization. Where a shift exists, it must be predictable and reproducible within an acceptable narrow error band. The above result confirmed that stabilization of TCO occurred the first twenty-four hours at temperature.

Thermal Stability of Sensitivity

The FSO at 300ºC of the six known good transducers consistently dropped to about 50% of the room temperature FSO as shown in the representative graph of Figure 5. The repeatability of the FSO in Figure 5 is an indication of the stability of the transducer sensitivity. This is further shown in Figure 7 for clarity. It is seen that the sensitivity of the representative transducer at room temperature is 25.83 μV/V/psi, which drops to about 13 μV/V/psi and 10 μV/V/psi at 300ºC and 400ºC, respectively.

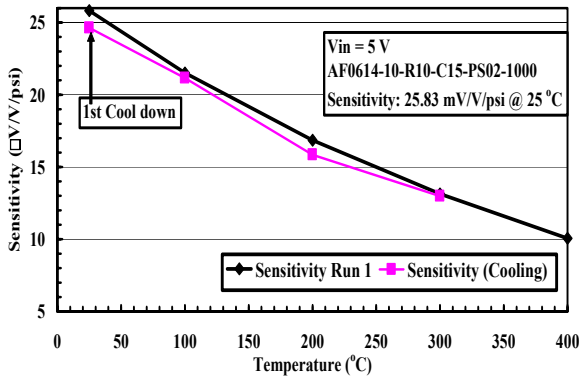

Figure 7: Representative temperature effect on sensitivity depicts the stability and reproducibility after maiden AST run. The drop in sensitivity is about 50% at 300ºC and 61% at 400ºC.

This represents a 50% and 61% drop in strain sensitivity at 300ºC and 400ºC, respectively. While variations in room temperature sensitivity have been observed across transducers having sensors that were fabricated from the same wafer, the temperature coefficient of sensitivity (TCS) have largely remained the same. The variation in room temperature sensitivity can be explained on the basis of variations in diaphragm thickness across the wafer during batch fabrication by deep reactive ion etching (DRIE). In cases where variations in sensitivity still exist even where the diaphragm thickness is the same, we surmise it is caused by the deep circular notch ("trench") that we observe to form at the corner between the diaphragm and the wall as a result of the enhanced DRIE that makes the diaphragm thinner than the base. Since we have observed that the notch is non uniform from across sensors, sensitivity will vary among transducers.

Thermal Stability of Resistance

The initial output resistance, R_o, of the sensor is a function of epilayer impurity concentration and is influenced by the impurity and phonon scattering carriers at lower and higher temperatures, respectively. Generally, in the lower temperature impurity scattering regime, the increasing density of the ionized carriers in the conduction band result in lowering of the resistivity. This results in the drop in the output resistance, as shown in the representative experimental graph of Figure 8 that compares the effect of temperature on the R_o of the tested transducers with that from other transducers that have epilayers of different nitrogen doping levels. As the temperature increases further, phonon scattering begins to dominate the carrier transport, leading to decreased conductivity (i.e. increased resistance) [12]. For epilayer with high impurity concentration as seen in Figure 8, full carrier ionization occurs at higher temperature than it does in the epilayer with lower concentration. Thus the minimum output resistance occurs at higher temperature.

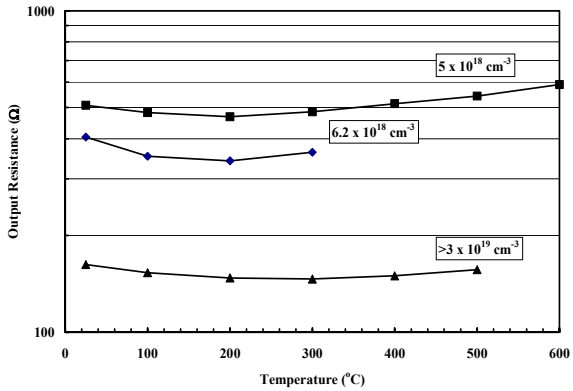

Figure 8: Representative plots of the bridge output resistance as function of temperature for selected n-type epilayer doping levels.

In piezoresistive silicon, full ionization typically takes place at lower than room temperature due to its low energy band gap (1.12 eV) [10]. However, as can be seen in Figure 8, the same is not the case for n-type 6H-SiC piezoresistive SiC which has a band gap of 3.03 eV [15]. The result is that in piezoresistive SiC, the temperature coefficient of

resistivity (TCR) between 25 and 600ºC mostly have bi-modal characteristics (i.e. strongly dominated by impurity and phonon scattering regimes at lower and higher temperatures, respectively) for a wide range of the impurity concentration. This bi-modal non-linear behavior makes on-chip temperature compensation a difficult challenge for piezoresistive SiC devices.

Conclusion

The AST performed in this work represents the first effort to systematically measure and develop reliability criteria of single crystal pressure transducers targeted for long duration use at temperatures above the capability of silicon-based MEMS devices. FEA was used to optimize the MEMS-DCA package design, thus allowing for a successful de-coupling of the thermomechanical stress from high CTE package components to the sensors. We have established benchmark reliability criteria for SiC pressure transducers for 300ºC applications on the basis of the thermal stability of critical operational parameters. From this reliability evaluation, we have validated the stability and reliability of fully packaged 6H-SiC pressure sensors for over 130 hours operation at 300ºC.

Acknowledgement

The fabrication and packaging of this project is funded by the Glennan Microsystems Initiative under contract number NAS3-03133 and the AST is funded under NASA's Intelligent Propulsion Systems Foundation Technology element under the Ultra-Efficient Engine Technology project. Author RSO thanks members of the technical staff of the NASA Sensors and Electronics Technology Branch for their support. Author ES thanks Prof. E. Madenci of the University of Arizona for performing the finite element stress analysis.

References

[1] Alexandar's Gas and Oil Connections, News and Trends: North America, vol. 8, Issue 13, 2003.

[2] International Civil Aviation Organization Standards: Annex 16 - *Environmental Protection, Volume II - Aircraft Engine Emissions*, 1999.

[3] J. von Berg, R. Ziermann, W. Reichert, E. Obermeier, M. Eickhoff, G. Krotz, U. Thoma, C. Cavalloni, and J.P. Nendza, 4th International High Temperature Electronics Conference, p. 45 – 249, 1998.

[4] Alex A. Ned, Robert S. Okojie, and Anthony D. Kurtz, "6H-SiC Pressure Sensor Operation at 600ºC," Trans. 4th Intl. High Temp. Elect. Conf., p. 257-260, 1998.

[5] Robert S. Okojie, Glenn M. Beheim, George J. Saad, and Ender Savrun, "Characteristics of a Hermetic 6H-SiC Pressure Sensor at 600ºC," Proc. 39th AIAA Mtg., Paper No. 2001-4652, 2001.

[6] N.V. Chidambaram, Proceedings 41st Electronic Components and Technology Conference, May 11-16, p. 877 – 882, 1991.

[7] S. Michaelides, S.K. Sitaraman, IEEE Transactions on Advanced Packaging, Vol. 22, Issue: 4 , p.:602 – 613, 1999.

[8] Robert S. Okojie, Patent pending

[9] Ender Savrun, and Wayne R. Johnson "Aluminum Nitride Packages for High-Power, High-Temperature Electronics," Sienna Technical Report No. 982, NASA Contract No. NAS3-99046, 1999.

[10] ANSYS, Inc. Global Headquarters, Southpointe 275 Technology Drive, Canonsburg, PA 15317.

[11] S. M. Sze, Semiconductor Devices: Physics and Technology, John Wiley and Sons, New York, 1985.

[12] B. E. Streetman. Solid State Electronic Devices, 3rd Ed. Prentice Hall, p. 86-7, 1990.

[13] Cree, Inc, 4600 Silicon Drive, Durham, NC 27703

[14] Robert S. Okojie, Alex A. Ned, and Anthony D. Kurtz, The Intl. Conf. Solid. State Sensors Actuators-97, Digest of Tech. Papers, v.2, p.1407-1409, 1997.

[15] Cree, Inc. Silicon Carbide Substrates Product Specification Sheet October 2003.